Review

Review of two-phase critical flow models and investigation of the relationship between choking, premature CHF, and CHF in micro-channel heat sinks

Sung-Min Kim [a], Issam Mudawar [b],*

[a] School of Mechanical Engineering, Sungkyunkwan University, 300 Cheoncheon-dong, Suwon 400-746, Republic of Korea
[b] Purdue University Boiling and Two-Phase Flow Laboratory (PU-BTPFL), Mechanical Engineering Building, 585 Purdue Mall, West Lafayette, IN 47907-2088, USA

ABSTRACT

Two-phase micro-channel heat sinks are known to exhibit several anomalies that are far less prevalent in macro-channels. High pressure drop in micro-channels is associated with appreciable compressibility, caused by strong variations of specific volumes of vapor and liquid with pressure, and flashing, which is the result of strong variations of enthalpies of vapor and liquid with pressure, and appreciable compressibility and flashing contribute to a high likelihood of two-phase choking. Another concern is two-phase flow instabilities, which are often associated with intense pressure oscillations. These instabilities are rooted in both two-phase compressibility and the use of parallel flow channels. A third concern is how choking and instabilities influence critical heat flux (CHF), including the possibility of triggering premature CHF. This study will review critical flow models and examine any relationship among choking, instabilities, premature CHF and CHF in micro-channel heat sinks. Different critical flow models are first assessed against published data for flow through pipes, short tube orifices, and short nozzles. The same models are then compared to previous experimental premature CHF and CHF data for micro-channel heat sinks. It is shown both can be associated with choking at low pressures, especially in heat sinks with very small hydraulic diameters.

© 2015 Elsevier Ltd. All rights reserved.

Contents

---

* Corresponding author. Tel.: +1 (765) 494 5705; fax: +1 (765) 494 0539.
  E-mail address: mudawar@ecn.purdue.edu (I. Mudawar).
  URL: https://engineering.purdue.edu/BTPFL (I. Mudawar).

Nomenclature

A	flow area
Bo	Boiling number, q''_H/Gh_{fg}
Ca	Capillary number, $Ca = (\mu_f\,G)/(\rho_f\sigma)$
c_p	specific heat at constant pressure
D	tube diameter
D_h	hydraulic diameter
G	mass velocity
g	gravitational acceleration
G_c	critical (choking) mass velocity
h	enthalpy
h_{fg}	latent heat of vaporization
L	heated length of channel
P	pressure
P_c	pressure at critical cross-section
P_{crit}	critical pressure (22.06 MPa for water)
P_F	wetted perimeter of channel
P_H	heated perimeter of channel
P_R	reduced pressure, $P_R = P/P_{crit}$
q''_{base}	heat flux averaged over base of heat sink
q''_{CHF}	critical heat flux
q''_H	effective heat flux averaged over heated perimeter of channel
q''_m	averaged heat flux in experimental data
q''_{P-CHF}	premature critical heat flux
Re_{fo}	liquid-only Reynolds number, $Re_{fo} = GD_h/\mu_f$
s	entropy
s_{fg}	entropy difference between saturated vapor and saturated liquid
S_r	slip ratio, $S_r = u_g/u_f$
T	temperature
t	time
u	mean velocity
u_i	interfacial velocity
v	specific volume

v_{fg}	specific volume difference between saturated vapor and saturated liquid
W	mass flow rate
We_{fo}	liquid-only Weber number, $We_{fo} = (G^2D_h)/(\rho_f\sigma)$
We_L	Weber number based on channel's heated length, $We_L = (G^2L)/(\rho_f\sigma)$
x	flow quality
x_{di}	dryout incipience quality
x_e	thermodynamic equilibrium quality
X_{tt}	Lockhart–Martinelli parameter based on turbulent liquid–turbulent vapor flow
z	stream-wise coordinate

Greek symbols

α	void fraction
β	volumetric thermal expansion coefficient
Γ_{fg}	evaporation mass transfer rate per unit channel length
μ	dynamic viscosity
ρ	density
ρ'	momentum density
$\bar{\rho}$	mixture density
σ	surface tension
τ	shear stress
τ_F	shear stress over wetted perimeter of channel
θ	channel inclination angle

Subscripts

f	saturated liquid
g	saturated vapor
i	interfacial
in	channel inlet
sub	subcooling
0	stagnation

1. Introduction

1.1. Two-phase choking for different flow configurations

Choked flow is encountered in many flow devices such as throttling valves and nozzles, and systems such as nuclear reactors. Also referred to as critical flow, choked flow is commonly encountered when decreasing downstream pressure. Initially, this decrease causes an increase in the flow rate, and choking is achieved when further reduction of the downstream pressure no longer affects the flow rate. Critical flow is, therefore, an important design parameter dictating the maximum flow rate for a device or system.

Because of high pressure drop, critical flow is often associated with phase change, which explains the emphasis many researchers have placed on two-phase critical flow for many decades. Many of these studies concern choking in a pipe [1–6], where maximum flow rate is measured in response to a sudden crack or high pressure drop from a pipe; the vast majority of these studies concern safe design of nuclear reactor thermal–hydraulics systems. Other studies on two-phase critical flow include short tube orifices [7,8], orifices [7,9,10], short nozzles [7,11], diverging nozzles [12], and converging–diverging nozzles [7,13]. The flow is choked at the critical cross-section, which is usually the minimum downstream cross-section as shown in Fig. 1. For example, the critical cross-section in an orifice, nozzle, or converging–diverging nozzle is the throat, while it is the pipe exit for a straight pipe.

1.2. Two-phase choking in micro-channels

Two-phase flow in micro-channel heat sinks has recently received significant attention for high-flux applications. Small diameter in these devices is key to achieving high heat transfer coefficients. However, small diameter can greatly increase pressure drop, which raises the likelihood of choking. The risk of choking in micro-channel heat sinks was first addressed by Bowers and Mudawar [14–16], who compared both experimentally and analytically the performances of two different multi-channel heat sinks using R113 as working fluid. One heat sink contained circular micro-channels with D_h = 0.51 mm and the other mini-channels with D_h = 2.50 mm; the two heat sinks featured fairly equal total wetted areas. Fig. 2 compares the variations of pressure drop across the two heat sinks with base heat flux. The pressure drop is both relatively small and fairly constant for both heat sinks at low heat fluxes. But once boiling is initiated in the channels, pressure drop escalates rapidly in the micro-channel heat sink with increasing heat flux, compared to a much milder increase in the mini-channel heat sink. Bowers and Mudawar explained these trends by property variations along the channel. High pressure drop in micro-channel heat sinks is associated with appreciable compressibility, caused by strong variations of specific volumes of vapor and liquid with pressure, and flashing, which is the result of strong variations of enthalpies of vapor and liquid with pressure. Additionally, high compressibility and flashing contribute to a high likelihood of two-phase choking.
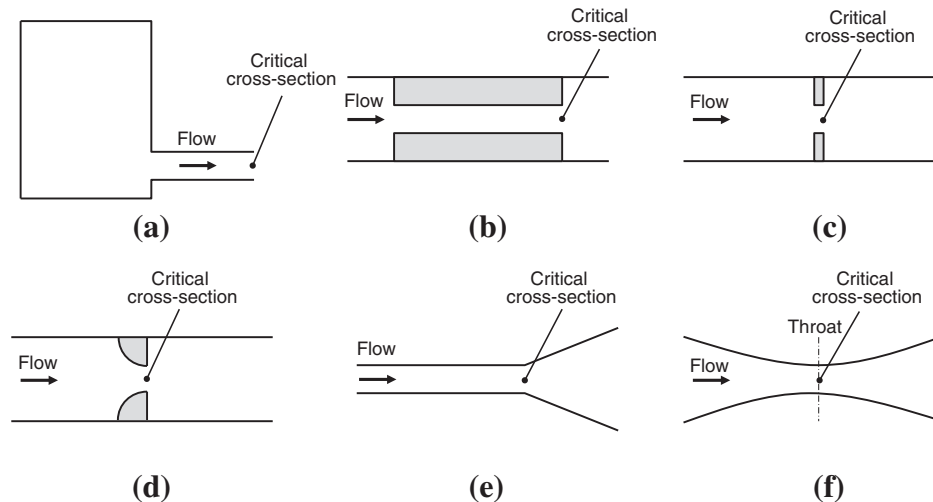
Fig. 1. Two-phase critical flow through (a) a pipe extending from a reservoir, (b) short tube orifice, (c) orifice, (d) short nozzle, (e) diverging nozzle, and (f) converging–diverging nozzle.
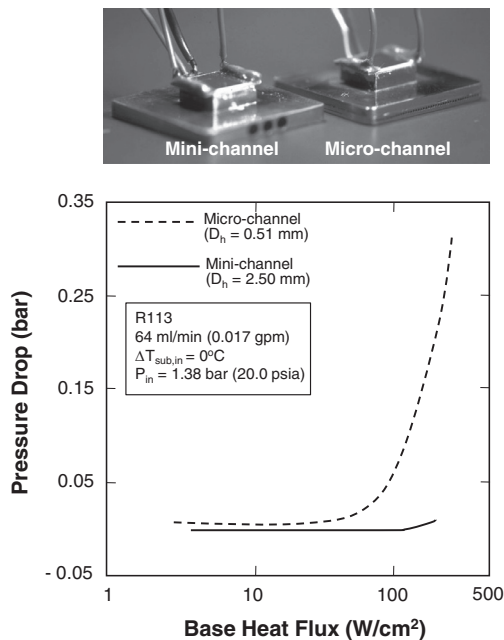

Fig. 2. Comparison of pressure drop characteristics for R113 in micro-channel and mini-channel heat sinks with identical inlet conditions. (Adapted from [14]).

Overall, choking is far more important to two-phase than single-phase systems, for it is associated with a relatively high critical flow velocity (equal to sonic velocity) for single-phase flow, compared to a much lower velocity for two-phase flow [14–18]. Therefore, choking can constitute a serious limit to the cooling performance of two-phase micro-channel heat sinks.

1.3. Pressure drop instabilities and premature Critical Heat Flux (CHF) in parallel micro-channels

Aside from inducing the afore-mentioned strong compressibility and flashing effects, vapor formation along micro-channels also induces complex flow instabilities. While flow instabilities are a common concern in all types of two-phase systems [19,20], they are especially problematic for micro-channels heat sinks. For instabilities in these devices are both more complex and sometimes associated with intense pressure variations. These instabilities are rooted in both two-phase compressibility and use of multiple parallel flow channels. Two types of flow instabilities have been identified in micro-channel heat sinks [21]: (1) severe pressure drop oscillation and (2) mild parallel channel instability. The first is the result of communication of compressible volume in the heat sink with that in the rest of the flow loop. As illustrated in Fig. 3(a), the severe pressure oscillation is associated with the spatial boundary between the single-phase liquid and two-phase regions in all channels of the heat sink oscillating back and forth in unison between the inlet and outlet, resulting in large amplitude pressure variations. An effective means to mitigating the severe pressure drop oscillation is to install throttling valves both upstream and downstream of the heat sink in order to dampen the communication of compressibility effects between the heat sink and rest of the flow loop. With effective throttling, only the second mild parallel channel instability is encountered. This instability takes the form of random fluctuations of the boiling boundary between the parallel micro-channels as illustrated in Fig. 3(b). Because of the relatively small amplitude of pressure fluctuations, this instability is mild enough to be tolerated during normal cooling system operation.

A key contributor to flow instabilities in micro-channel heat sinks is high heat flux. Fig. 4 shows an extreme form of severe pressure oscillation at high heat flux in a micro-channel heat sink using HFE-7100 as working fluid [22]. Oscillation of the boiling boundary in this case is strong enough to force vapor backwards into the inlet plenum, inducing Critical Heat Flux (CHF) prematurely in the upstream region of the heat sink.

1.4. Departure from Nucleate Boiling (DNB), dryout and dryout incipience in micro-channels

Critical heat flux is arguably the most important heat transfer limit for heat-flux controlled heat transfer devices, including micro-channel heat sinks. It is generally associated with an appreciable reduction in the local heat transfer coefficient due to interruption of liquid access to the heated wall. CHF occurrence is accompanied by a sudden appreciable rise in the wall temperature, which, depending on the cooling fluid and operating conditions, may result in catastrophic failure of the cooling device.

Two different CHF mechanisms have been encountered in micro-channel heat sinks: Departure from Nucleate Boiling (DNB)
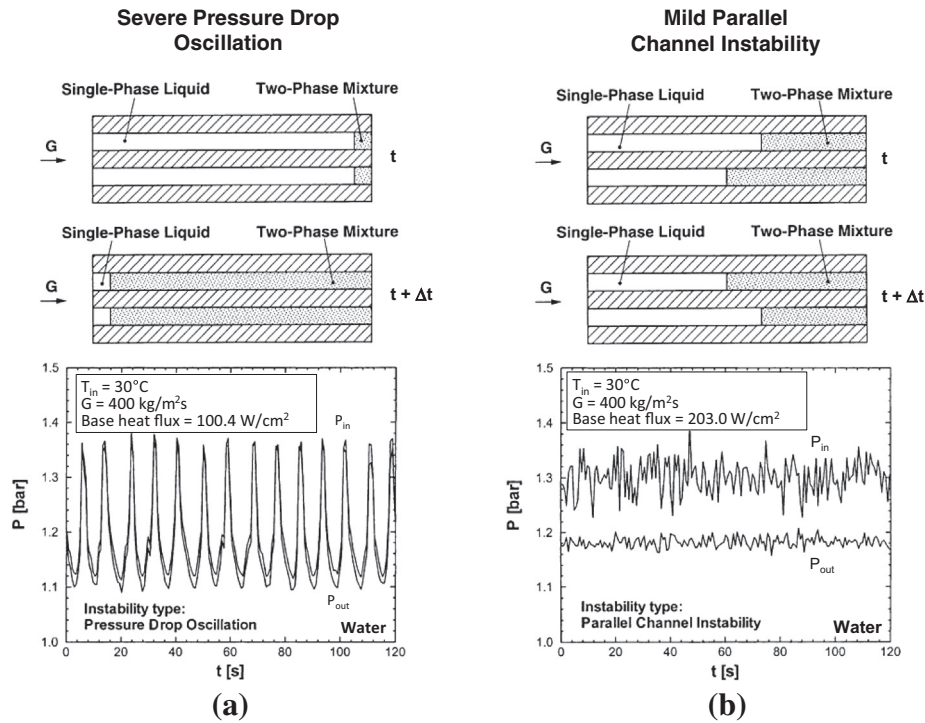
Fig. 3. Top view depictions of two neighboring micro-channels, and temporal records of inlet and outlet pressures during (a) severe pressure drop oscillation and (b) mild parallel channel instability. (Adapted from [21]).
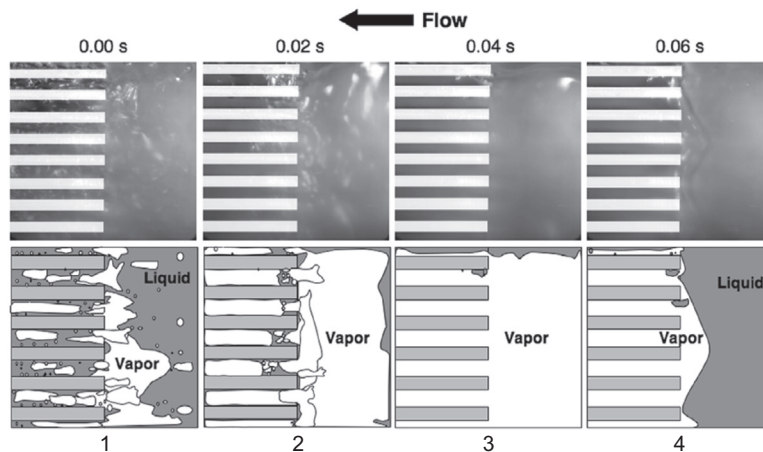

Fig. 4. Premature CHF and flow oscillations for HFE-7100 in heat sink with D_h = 415.9 μm for T_{in} = 0 °C, G = 670 kg/m² s and q''_{base} > 250.0 W/cm²: (1) initial vapor pocket buildup in upstream plenum, (2) growth of vapor mass, (3) complete blockage of inlet plenum by vapor mass, and (4) purging of vapor mass along micro-channels. (Adapted from [22]).

and dryout. Fig. 5(a) illustrates DNB occurrence in a micro-channel heat sink with D_h = 334.1 μm when using HFE-7100 as working fluid [22]. In this case, bubbles quickly coalesce into a continuous vapor blanket along the channel wall, even while liquid is quite abundant in the core. The thermally insulating blanket prevents any further contact of liquid with the channel wall, triggering a sudden unsteady rise in the heat sink temperature. DNB is more commonly encountered at high mass velocities and high inlet sub-coolings, especially in heat sinks with small length-to-diameter ratios [22]. On the other hand, dryout is generally encountered at low mass velocities, saturated or slightly subcooled inlet conditions, and large length-to-diameter ratios. This form of CHF occurs in the annular regime as the liquid film is fully consumed by evaporation, exposing the wall to the vapor core.

Another important cooling limit is dryout incipience, which constitutes a precursor to dryout. Dryout incipience is encountered when local portions of the annular liquid film begin to dry out. This is shown in Fig. 5(b) for flow boiling of R134a in a heat sink containing rectangular micro-channels [23,24].

1.5. Objectives of study

While critical flow is important to all types of two-phase systems, it is of special concern for devices containing small channels. Both critical flow and instabilities (especially severe pressure oscillation) in two-phase micro-channel heat sinks are associated with compressibility effects. Furthermore, premature CHF appears to be

associated with difficulty passing liquid through the parallel micro-channels, and may therefore be associated with critical flow.

This study will review critical flow models and examine any relationships among critical flow, instabilities, premature CHF and CHF in micro-channel heat sinks. Specific objectives of the study are to:

(1) Provide a comprehensive review of two-phase critical flow models.
(2) Assess the predictive accuracy of two-phase critical flow models against published data for flow through pipes, short tube orifices, and short nozzles.
(3) Assess the relationship among two-phase critical flow, CHF, premature CHF, and dryout incipience for micro-channel heat sinks.

2. Two-phase critical flow models based on Separated Flow Model (SFM)

The Separated Flow Model (SFM) differs from the simpler Homogenous Flow Model (HEM) discussed in the next section primarily in its flexibility in representing the two phases with their individual properties and velocities. The simplest of separated flow models, the so-called Slip Flow Model, assumes one-dimensional flow with uniform velocity within each phase, while allowing for differences between the phase velocities. As discussed below, this model has been used to derive several competing relations for two-phase critical flow. Following are key assumptions of the steady Slip Flow Model:

(1) Vapor and liquid phases are separated from one another and occupy identifiable portions of the flow area.
(2) Velocity profile is uniform across each phase.
(3) Vapor–liquid interface is smooth.
(4) Pressure is uniform across the channel's cross-sectional area (i.e., $P_g = P_f = P$).
(5) Thermophysical properties of the individual phases are based on local saturation pressure.

(6) Thermodynamic equilibrium is maintained along the channel, i.e., $x = x_e$ in the two-phase region ($0 \leqslant x_e \leqslant 1$).

Fig. 6 illustrates momentum and force components for two-phase flow in a channel based on the Slip Flow Model. Momentum conservation for the vapor and liquid layers in a channel differential control volume of length Δz is given, respectively, as

$$\frac{d}{dz}(\rho_g u_g^2 A_g) - \Gamma_{fg} u_i = -\alpha A \frac{dP}{dz} - \tau_{F_g} P_{F_g} - \tau_i P_i - \rho_g g \alpha A \sin\theta \qquad (1)$$

and

$$\frac{d}{dz}(\rho_f u_f^2 A_f) + \Gamma_{fg} u_i = -(1-\alpha)A \frac{dP}{dz} - \tau_{F_f} P_{F_f} + \tau_i P_i - \rho_f g(1-\alpha)A \sin\theta, \qquad (2)$$

where Γ_{fg}, u_i, τ_{Fg}, τ_{Ff}, τ_i, P_{Fg}, P_{Ff}, and P_i are, respectively, the rate of mass transfer due to evaporation along the vapor–liquid interface, interfacial axial velocity, shear stress between the vapor layer and the wall, shear stress between the liquid layer and the wall, interfacial shear stress, portion of channel's perimeter covered with vapor, portion of channel's perimeter covered with liquid, and interfacial perimeter. Introducing the definitions for flow quality, $x = W_g/W$, and void fraction, $\alpha = A_g/A$, reduces the axial momentum terms for the vapor and liquid layers, respectively, to the following.

$$\rho_g u_g^2 A_g = \frac{x^2 W^2}{\rho_g \alpha A} = \frac{x^2 G^2 A}{\rho_g \alpha}, \qquad (3)$$

and

$$\rho_f u_f^2 A_f = \frac{(1-x)^2 W^2}{\rho_f (1-\alpha) A} = \frac{(1-x)^2 G^2 A}{\rho_f (1-\alpha)}. \qquad (4)$$

Substituting Eq. (3) into Eq. (1), and Eq. (4) into Eq. (2), and adding resulting relations yields

$$G^2 \frac{d}{dz} \left[\frac{x^2 A}{\rho_g \alpha} + \frac{(1-x)^2 A}{\rho_f (1-\alpha)} \right] = -A \frac{dP}{dz} - (\tau_{F_g} P_{F_g} + \tau_{F_f} P_{F_f})$$
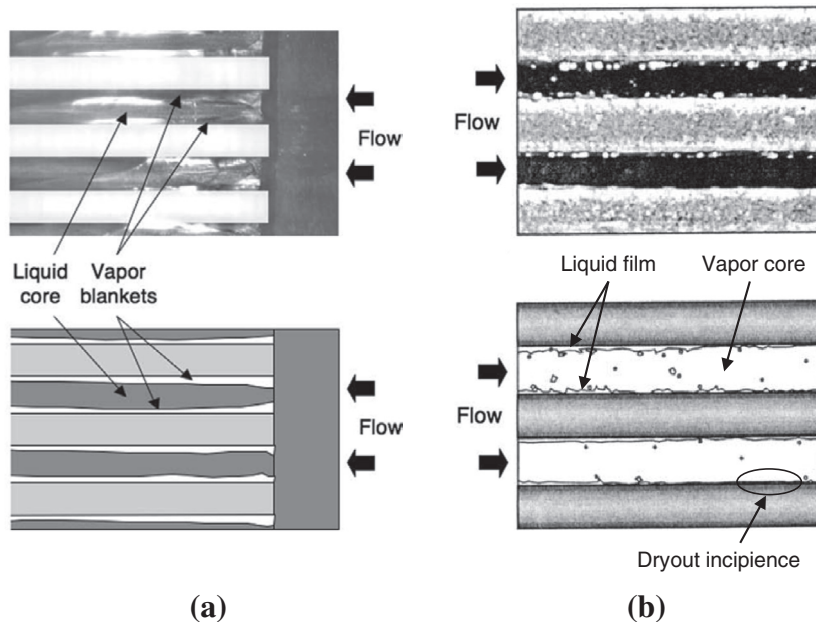$$- [\rho_g \alpha + \rho_f (1-\alpha)] g A \sin\theta. \qquad (5)$$

(a)   **(b)**

Fig. 5. CHF mechanisms in micro-channel heat sinks. (a) DNB for HFE-7100 in heat sink with $D_h = 334.1\ \mu m$ for $T_{in} = 0\ °C$, $G = 1341\ kg/m^2\ s$ and $q''_{base} = 325.8\ W/cm^2$ (adapted from [22]). (b) Dryout incipience for R134a in heat sink with $D_h = 348.9\ \mu m$ for $x = 0.68$, $G = 128\ kg/m^2\ s$ and $q''_{base} = 31.6\ W/cm^2$ (adapted from [23,24]).
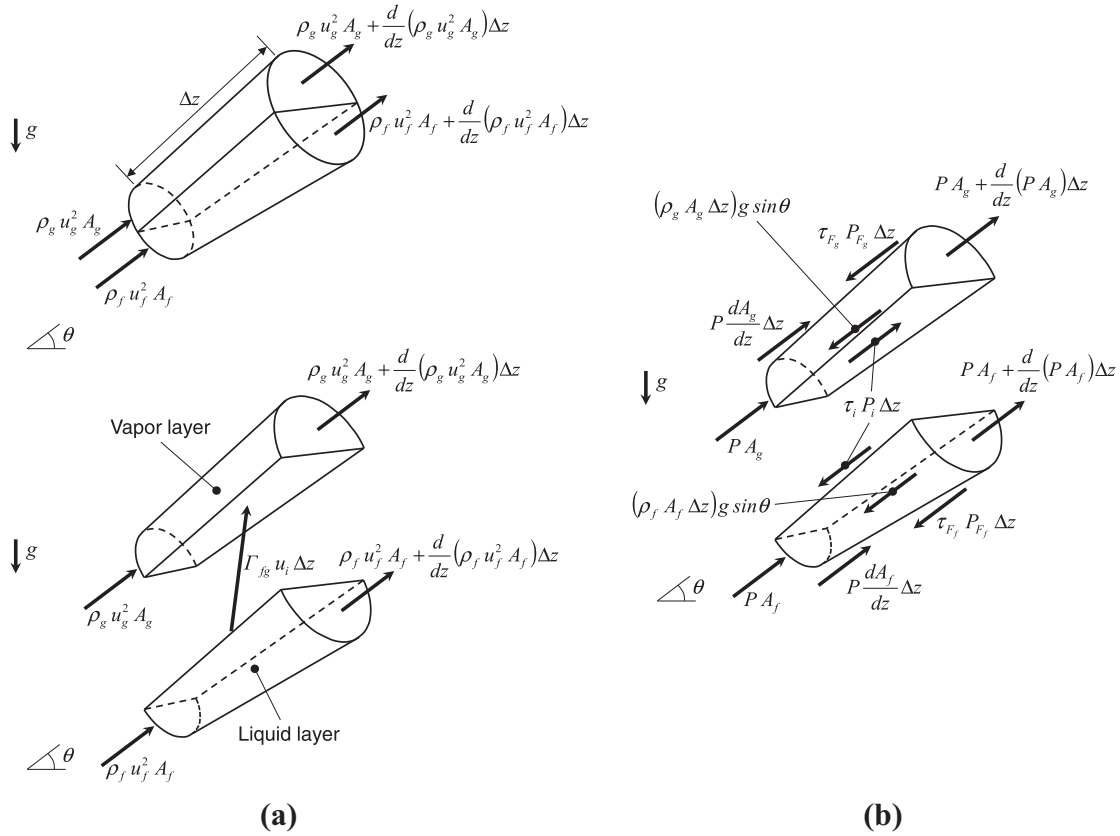
Fig. 6. (a) Momentum components for combined two-phase flow and for individual layers. (b) Force components for individual layers.

For a constant flow area, Eq. (5) can be simplified into

$$G^2 \frac{d}{dz}\left(\frac{1}{\rho'}\right) = -\frac{dP}{dz} - \frac{\tau_F P_F}{A} - \bar{\rho} g \sin\theta, \tag{6}$$

where

$$\tau_F P_F = \tau_{F_g} P_{F_g} + \tau_{F_f} P_{F_f}, \tag{7}$$

and the momentum density, ρ', and mixture density, $\bar{\rho}$, are defined, respectively, as

$$\frac{1}{\rho'} = \frac{x^2}{\rho_g \alpha} + \frac{(1-x)^2}{\rho_f(1-\alpha)}, \tag{8}$$

and

$$\bar{\rho} = \rho_g \alpha + \rho_f(1-\alpha). \tag{9}$$

Based on assumption (5), the convective term in Eq. (6) can be expressed as

$$\frac{d}{dz}\left(\frac{1}{\rho'}\right) = \left[\frac{d}{dP}\left(\frac{1}{\rho'}\right)\right]\frac{dP}{dz}. \tag{10}$$

Substituting Eq. (10) into Eq. (6) yields

$$-\frac{dP}{dz} = \frac{\frac{\tau_F P_F}{A} + \bar{\rho} g \sin\theta}{1 + G^2\left[\frac{d}{dP}\left(\frac{1}{\rho'}\right)\right]}. \tag{11}$$

Following Fauske's [2] assumption that the pressure gradient has a finite maximum value at the choking point, maximum pressure gradient is achieved by setting the denominator of Eq. (11) equal to zero, which yields the following relation for critical mass velocity

$$G_c = \left[-\frac{d}{dP}\left(\frac{1}{\rho'}\right)\right]^{-1/2} = \left\{-\frac{d}{dP}\left[\frac{v_g x^2}{\alpha} + \frac{v_f(1-x)^2}{(1-\alpha)}\right]\right\}^{-1/2}. \tag{12}$$

Differentiating terms in Eq. (12) yields

$$\frac{d}{dP}\left[\frac{v_g x^2}{\alpha} + \frac{v_f(1-x)^2}{(1-\alpha)}\right] = \frac{x^2}{\alpha}\frac{dv_g}{dP} + \frac{2v_g x}{\alpha}\frac{dx}{dP} - \frac{v_g x^2}{\alpha^2}\frac{d\alpha}{dP}$$
$$+ \frac{(1-x)^2}{(1-\alpha)}\frac{dv_f}{dP} - \frac{2v_f(1-x)}{(1-\alpha)}\frac{dx}{dP}$$
$$+ \frac{v_f(1-x)^2}{(1-\alpha)^2}\frac{d\alpha}{dP}. \tag{13}$$

Then, the critical mass velocity is given by

$$G_c = \left\{-\left[\frac{x^2}{\alpha}\frac{dv_g}{dP} + \frac{(1-x)^2}{(1-\alpha)}\frac{dv_f}{dP} + \left(\frac{2v_g x}{\alpha} - \frac{2v_f(1-x)}{(1-\alpha)}\right)\frac{dx}{dP}\right.\right.$$
$$\left.\left. - \left(\frac{v_g x^2}{\alpha^2} - \frac{v_f(1-x)^2}{(1-\alpha)^2}\right)\frac{d\alpha}{dP}\right]\right\}^{-1/2}. \tag{14}$$

The derivatives dv_g/dP and dv_f/dP in Eq. (14) can be easily evaluated from saturated property tables. The derivative dx/dP, which is related to interfacial mass transfer between the phases, can be evaluated under assumptions of isenthalpic or isentropic flow, or based on thermodynamic relations as will be discussed later. The derivative of void fraction with respect to pressure, $d\alpha/dP$, can be evaluated using the void fraction relation of Baroczy [25],

$$\alpha = \left[1 + \left(\frac{1-x}{x}\right)^{0.74}\left(\frac{v_f}{v_g}\right)^{0.65}\left(\frac{\mu_f}{\mu_g}\right)^{0.13}\right]^{-1}. \tag{15}$$

From Eq. (15), the derivative of α with respect to pressure can be expressed as

$$\frac{d\alpha}{dP} = \frac{d\alpha}{dx}\frac{dx}{dP} + \frac{d\alpha}{dv_f}\frac{dv_f}{dP} + \frac{d\alpha}{dv_g}\frac{dv_g}{dP} + \frac{d\alpha}{d\mu_f}\frac{d\mu_f}{dP} + \frac{d\alpha}{d\mu_g}\frac{d\mu_g}{dP}, \quad (16)$$

where the derivatives $d\mu_g/dP$ and $d\mu_f/dP$ can be calculated from saturated property tables.

The void fraction relation can also be correlated using the Lockhart–Martinelli parameter [26]. Wallis [18] formulated the relation

$$\alpha = (1 + X_{tt}^{0.8})^{-0.378}, \quad (17)$$

by fitting void fraction data, where the Lockhart–Martinelli parameter is based on the combination of turbulent liquid and turbulent vapor flows,

$$X_{tt} = \left(\frac{1}{x} - 1\right)^{0.9} \left(\frac{v_f}{v_g}\right)^{0.5} \left(\frac{\mu_f}{\mu_g}\right)^{0.1}. \quad (18)$$

The derivative of Eq. (17) with respect to pressure can be expressed as

$$\frac{d\alpha}{dP} = \frac{d\alpha}{dX_{tt}}\left(\frac{dX_{tt}}{dx}\frac{dx}{dP} + \frac{dX_{tt}}{dv_f}\frac{dv_f}{dP} + \frac{dX_{tt}}{dv_g}\frac{dv_g}{dP} + \frac{dX_{tt}}{d\mu_f}\frac{d\mu_f}{dP} + \frac{dX_{tt}}{d\mu_g}\frac{d\mu_g}{dP}\right). \quad (19)$$

The void fraction in Eq. (12) can be related to the slip ratio, S_r, which is defined as the ratio of vapor velocity to liquid velocity, $S_r = u_g/u_f$. Using the definition of flow quality,

$$x = \frac{W_g}{W} = \frac{\rho_g u_g A_g}{\rho_g u_g A_g + \rho_f u_f A_f} = \frac{1}{1 + \frac{\rho_f}{\rho_g}\frac{u_f}{u_g}\frac{A_f}{A_g}} = \frac{1}{1 + \frac{\rho_f}{\rho_g}\frac{1}{S_r}\left(\frac{1-\alpha}{\alpha}\right)}, \quad (20)$$

yields the following relation for void fraction as a function of slip ratio, specific volume ratio, and flow quality,

$$\alpha = \frac{1}{1 + S_r\frac{v_f}{v_g}\left(\frac{1-x}{x}\right)}. \quad (21)$$

Substituting Eq. (21) into Eq. (8) yields

$$\frac{1}{\rho'} = v_g x^2 + v_f S_r x(1-x) + \frac{v_g(1-x)x}{S_r} + v_f(1-x)^2. \quad (22)$$

Differentiating Eq. (22) with respect to pressure yields

$$\frac{d}{dP}\left(\frac{1}{\rho'}\right) = x^2\frac{dv_g}{dP} + 2v_g x\frac{dx}{dP} + S_r x(1-x)\frac{dv_f}{dP} + v_f x(1-x)\frac{dS_r}{dP}$$
$$+ v_f S_r(1-2x)\frac{dx}{dP} + \frac{(1-x)x}{S_r}\frac{dv_g}{dP} - \frac{v_g(1-x)x}{S_r^2}\frac{dS_r}{dP}$$
$$+ \frac{v_g(1-2x)}{S_r}\frac{dx}{dP} + (1-x)^2\frac{dv_f}{dP} - 2v_f(1-x)\frac{dx}{dP}. \quad (23)$$

Then, from Eq. (12), the critical mass velocity is given by

$$G_c = \left\{-\left[\left(x^2 + \frac{x(1-x)}{S_r}\right)\frac{dv_g}{dP} + ((1-x)^2 + S_r x(1-x))\frac{dv_f}{dP}\right.\right.$$
$$+ \left(2v_g x + \frac{v_g(1-2x)}{S_r} + v_f S_r(1-2x) - 2v_f(1-x)\right)\frac{dx}{dP}$$
$$\left.\left.+ x(1-x)\left(v_f - \frac{v_g}{S_r^2}\right)\frac{dS_r}{dP}\right]\right\}^{-1/2}. \quad (24)$$

Fauske [2] and Moody [27] developed theoretical annular two-phase flow models to predict the critical flow rate. In both models, the slip ratio was expressed as a function of specific volume ratio. Fauske obtained $S_r = (v_g/v_f)^{1/2}$ by minimizing momentum density given by Eq. (22) in the critical cross-section, i.e., by setting

Table 1
Slip ratio relations.

Author/model	Slip ratio ($S_r = u_g/u_f$)
Fauske [2]	$(v_g/v_f)^{1/2}$
Moody [27], Zivi [28]	$(v_g/v_f)^{1/3}$
Homogeneous Equilibrium Model	1
Homogeneous Frozen Model	1

$$\frac{d(1/\rho')}{dS_r} = x(1-x)\left(v_f - \frac{v_g}{S_r^2}\right) = 0. \quad (25)$$

On the other hand, Moody obtained $S_r = (v_g/v_f)^{1/3}$ by maximizing two-phase flow rate as will be discussed later. The slip ratio of Moody is identical to that of Zivi [28], who minimized kinetic energy flux in the critical cross-section.

The slip ratio relations used in this study are summarized in Table 1. With either the Fauske or Moody formulations, the derivative of slip ratio with respect to pressure can be expressed as

$$\frac{dS_r}{dP} = \frac{dS_r}{dv_f}\frac{dv_f}{dP} + \frac{dS_r}{dv_g}\frac{dv_g}{dP}. \quad (26)$$

2.1. Fauske's relation for critical mass velocity

Substituting Fauske's [2] slip ratio relation, $S_r = (v_g/v_f)^{1/2}$, into Eq. (24) gives [2]

$$G_c = \left\{-\left[\left(x^2 + \frac{x(1-x)}{S_r}\right)\frac{dv_g}{dP} + \left((1-x)^2 + S_r x(1-x)\right)\frac{dv_f}{dP}\right.\right.$$
$$\left.\left.+ \left(2v_g x + \frac{v_g(1-2x)}{S_r} + v_f S_r(1-2x) - 2v_f(1-x)\right)\frac{dx}{dP}\right]\right\}^{-1/2}. \quad (27)$$

Since $dv_f/dP \ll dv_g/dP$ for relatively low pressures (up to 400 psia for steam-water), and $dx/dP = 0$ for two-phase flow without mass transfer (e.g., air–water flow), Eq. (27) can be simplified for low pressure adiabatic flow as

$$G_c = \left\{-\left[x^2 + \frac{x(1-x)}{S_r}\right]\frac{dv_g}{dP}\right\}^{-1/2}. \quad (28)$$

2.2. Moody's relation for critical mass velocity

Based on the assumption of isentropic two-phase annular flow through a nozzle, Moody [27] developed a simplified Slip Flow Model, where the liquid and vapor velocities are expressed, respectively, as

$$u_f = \frac{G(1-x)}{\rho_f(1-\alpha)}, \quad (29)$$

and

$$u_g = \frac{Gx}{\rho_g\alpha}. \quad (30)$$

For isentropic flow, the stagnation entropy is constant and given by

$$s_0 = s_f + xs_{fg}, \quad (31)$$

and the energy equation for adiabatic and frictionless flow (i.e., isentropic flow) is given by

$$h_0 = x\left(h_g + \frac{u_g^2}{2}\right) + (1-x)\left(h_f + \frac{u_f^2}{2}\right). \quad (32)$$

Combining the relations of phase velocities, Eqs. (29) and (30), stagnation properties, Eqs. (31) and (32), and void fraction, Eq. (21), yields the following relation for mass velocity,

$$G = \left\{ \frac{2\left[h_0 - h_f - \frac{h_{fg}}{s_{fg}}(s_0 - s_f)\right]}{\left[\frac{S_r(s_g - s_0)v_f}{s_{fg}} + \frac{(s_0 - s_f)v_g}{s_{fg}}\right]^2 \left[\frac{s_0 - s_f}{s_{fg}} + \frac{s_g - s_0}{S_r^2 s_{fg}}\right]} \right\}^{1/2}. \tag{33}$$

Since Eq. (33) is a function of pressure and slip ratio, this equation must satisfy the following relations at maximum flow condition,

$$\left.\frac{\partial G}{\partial S_r}\right|_P = 0. \tag{34}$$

and

$$\left.\frac{\partial G}{\partial P}\right|_{S_r} = 0. \tag{35}$$

The following relation for slip ratio at the maximum flow condition is obtained using Eq. (34),

$$S_r = \left(\frac{v_g}{v_f}\right)^{1/3}. \tag{36}$$

Then, the critical mass velocity can be obtained iteratively using Eqs. (33) and (35).

Moody [27] derived the following relation for critical mass velocity in terms of local static properties using Eqs. (33)–(35),

$$G_c = \left[-\frac{2(v_f + xv_{fg})}{a(ad + 2be)}\right]^{1/2}. \tag{37}$$

where

$$a = S_r v_f + x(v_g - S_r v_f), \tag{38a}$$

$$b = \frac{1}{S_r^2} + x\left(1 - \frac{1}{S_r^2}\right), \tag{38b}$$

$$d = \left[\frac{1}{S_r^2 s_{fg}}\frac{ds_g}{dP} - \frac{1}{s_{fg}}\frac{ds_f}{dP} - \frac{1}{S_r^4 s_{fg}}\frac{d}{dP}\left(s_{fg}S_r^2\right)\right]$$
$$+ x\left[\frac{1}{S_r^4 s_{fg}}\frac{d}{dP}\left(s_{fg}S_r^2\right) - \frac{1}{s_{fg}}\frac{ds_{fg}}{dP}\right], \tag{38c}$$

and

$$e = \left[s_{fg}\frac{d}{dP}\left(\frac{S_r v_f}{s_{fg}}\right) + \frac{S_r v_f}{s_{fg}}\frac{ds_g}{dP} - \frac{v_g}{s_{fg}}\frac{ds_f}{dP}\right]$$
$$+ x\left[s_{fg}\frac{d}{dP}\left(\frac{v_g}{s_{fg}}\right) - s_{fg}\frac{d}{dP}\left(\frac{S_r v_f}{s_{fg}}\right)\right], \tag{38d}$$

and the slip ratio is determined by Eq. (36).

3. Two-phase critical flow models based on Homogeneous Equilibrium Model (HEM)

The Homogeneous Equilibrium Model (HEM) treats a two-phase mixture as a pseudo fluid possessing properties that are uniform across the flow area. The model also assumes equal phase velocities and uniform velocity across the flow area. Since $S_r = 1$, Eq. (21) yields the following relation for void fraction,

$$\alpha = \frac{1}{1 + \frac{v_f}{v_g}\left(\frac{1-x}{x}\right)}. \tag{39}$$

Substituting Eq. (39) into Eq. (8) yields

$$\frac{1}{\rho'} = xv_g + v_f(1 - x). \tag{40}$$

Differentiating Eq. (40) with respect to pressure and substituting into Eq. (12) yields the following relation for HEM critical mass velocity,

$$G_c = \left\{-\left[x\frac{dv_g}{dP} + (1-x)\frac{dv_f}{dP} + (v_g - v_f)\frac{dx}{dP}\right]\right\}^{-0.5}. \tag{41}$$

3.1. Critical mass velocity for non-flashing two-phase flow

When interfacial mass transfer is negligible (i.e., $dx/dP = 0$), Eq. (41) can be reduced to the following relation for the Homogeneous Frozen (non-flashing) Model critical mass velocity,

$$G_c = \left\{-\left[x\frac{dv_g}{dP} + (1-x)\frac{dv_f}{dP}\right]\right\}^{-0.5}. \tag{42}$$

Eq. (42) was derived by Wallis [18] for homogeneous flow with negligible flashing.

The derivative of quality with respect to pressure, dx/dP, can be calculated using isenthalpic or isentropic assumptions, or by using thermodynamic relations.

3.2. Critical mass velocity for isenthalpic two-phase flow

For an isenthalpic process, enthalpy is constant, and

$$dh = d(h_f + xh_{fg}) = 0. \tag{43}$$

$$\frac{dx}{dP} = -\frac{1}{h_{fg}}\left(\frac{dh_f}{dP} + x\frac{dh_{fg}}{dP}\right), \tag{44}$$

which, when combined with Eq. (41), yields the following relation for critical mass velocity [29],

$$G_c = \left\{-\left[x\frac{dv_g}{dP} + (1-x)\frac{dv_f}{dP} - \frac{v_{fg}}{h_{fg}}\left(\frac{dh_f}{dP} + x\frac{dh_{fg}}{dP}\right)\right]\right\}^{-0.5}. \tag{45}$$

3.3. Critical mass velocity for isentropic two-phase flow

For an isentropic process, the entropy is constant, and

$$ds = d(s_f + xs_{fg}) = 0. \tag{46}$$

Rearranging Eq. (46) yields the variation of dx/dP along an isentropic path,

$$\frac{dx}{dP} = -\frac{1}{s_{fg}}\left(\frac{ds_f}{dP} + x\frac{ds_{fg}}{dP}\right). \tag{47}$$

Combining Eqs. (41) and (47) yields the following relation for critical mass velocity [29],

$$G_c = \left\{-\left[x\frac{dv_g}{dP} + (1-x)\frac{dv_f}{dP} - \frac{v_{fg}}{s_{fg}}\left(\frac{ds_f}{dP} + x\frac{ds_{fg}}{dP}\right)\right]\right\}^{-0.5}. \tag{48}$$

3.4. Determination of critical mass velocity for isentropic two-phase flow using thermodynamic relations

For an isentropic process, the thermodynamic relation $Tds = dh - vdP$ is reduced to

$$dh - vdP = d(h_f + xh_{fg}) - (v_f + xv_{fg})dP = 0. \tag{49}$$

Considering enthalpy as a function of temperature and pressure, the enthalpy changes for vapor and liquid can be expressed, respectively, as

$$dh_g = c_{p,g}dT, \tag{50}$$

and
$$dh_f = c_{p,f} dT + v_f (1 - \beta T) dP, \tag{51}$$

where β is the volumetric thermal expansion coefficient defined as

$$\beta = \frac{1}{v_f} \left. \frac{\partial v_f}{\partial T} \right|_P. \tag{52}$$

Notice that the pressure change term in Eq. (50) is neglected because it is much smaller than the temperature change term.

Using the Clapeyron equation,

$$\frac{dT}{dP} = \frac{T v_{fg}}{h_{fg}}, \tag{53}$$

and combining Eqs. (49)–(53) yields

$$\frac{dx}{dP} = \frac{v_f + x v_{fg}}{h_{fg}} - x c_{p,g} \frac{T v_{fg}}{h_{fg}^2} - \frac{(1-x)}{h_{fg}} \left[c_{p,f} \frac{T v_{fg}}{h_{fg}} + v_f (1 - \beta T) \right]. \tag{54}$$

Then, combining Eqs. (41) and (54) yields following relation for critical mass velocity,

Table 2
Two-phase critical flow models.

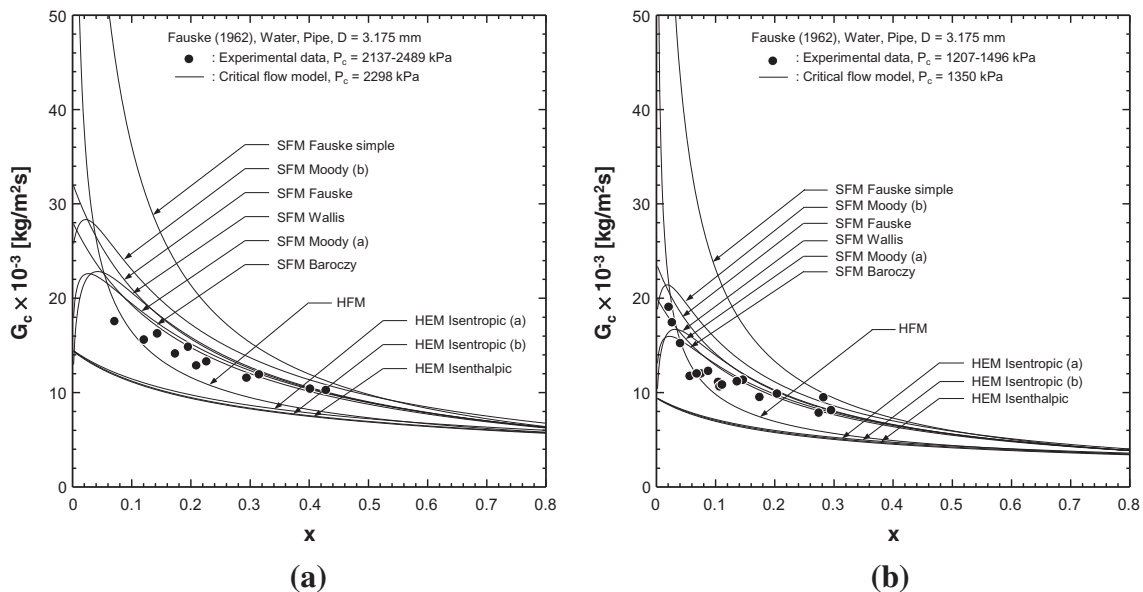|	Model	Equation
Slip Flow Models	SFM Baroczy	$G_c = \left\{ - \left[\frac{x^2}{\alpha} \frac{dv_g}{dP} + \frac{(1-x)^2}{(1-\alpha)} \frac{dv_f}{dP} + \left(\frac{2v_g x}{\alpha} - \frac{2v_f(1-x)}{(1-\alpha)} \right) \frac{dx}{dP} - \left(\frac{v_g x^2}{\alpha^2} - \frac{v_f(1-x)^2}{(1-\alpha)^2} \right) \frac{d\alpha}{dP} \right] \right\}^{-1/2}$ where $\alpha = \left[1 + \left(\frac{1-x}{x} \right)^{0.74} \left(\frac{v_f}{v_g} \right)^{0.65} \left(\frac{\mu_f}{\mu_g} \right)^{0.13} \right]^{-1}$
	SFM Wallis	$G_c = \left\{ - \left[\frac{x^2}{\alpha} \frac{dv_g}{dP} + \frac{(1-x)^2}{(1-\alpha)} \frac{dv_f}{dP} + \left(\frac{2v_g x}{\alpha} - \frac{2v_f(1-x)}{(1-\alpha)} \right) \frac{dx}{dP} - \left(\frac{v_g x^2}{\alpha^2} - \frac{v_f(1-x)^2}{(1-\alpha)^2} \right) \frac{d\alpha}{dP} \right] \right\}^{-1/2}$ where $\alpha = (1 + X_{tt}^{0.8})^{-0.378}$
	SFM Moody (a)	$G_c = \left\{ - \left[\left(x^2 + \frac{x(1-x)}{S_r} \right) \frac{dv_g}{dP} + ((1-x)^2 + S_r x(1-x)) \frac{dv_f}{dP} + \left(2v_g x + \frac{v_g(1-2x)}{S_r} + v_f S_r(1-2x) - 2v_f(1-x) \right) \frac{dx}{dP} + x(1-x) \left(v_f - \frac{v_g}{S_r^2} \right) \frac{dS_r}{dP} \right] \right\}^{-1/2}$ where $S_r = (v_g / v_f)^{1/3}$
	SFM Fauske [2]	$G_c = \left\{ - \left[(x^2 + \frac{x(1-x)}{S_r}) \frac{dv_g}{dP} + ((1-x)^2 + S_r x(1-x)) \frac{dv_f}{dP} + \left(2v_g x + \frac{v_g(1-2x)}{S_r} + v_f S_r(1-2x) - 2v_f(1-x) \right) \frac{dx}{dP} \right] \right\}^{-1/2}$ where $S_r = (v_g / v_f)^{1/2}$
	SFM Fauske simple [2]	$G_c = \left\{ - \left[x^2 + \frac{x(1-x)}{S_r} \right] \frac{dv_g}{dP} \right\}^{-1/2}$
	SFM Moody (b) [27]	$G_c = \left[- \frac{2(v_f + x v_{fg})}{a(ad + 2be)} \right]^{1/2}$ where a, b, d, and e are given by Eqs. (38a), (38b), (38c) and (38d), respectively
Homogeneous Equilibrium Models	HEM isenthalpic [29]	$G_c = \left\{ - \left[x \frac{dv_g}{dP} + (1-x) \frac{dv_f}{dP} - \frac{v_{fg}}{h_{fg}} \left(\frac{dh_f}{dP} + x \frac{dh_{fg}}{dP} \right) \right] \right\}^{-0.5}$
	HEM isentropic (a) [29]	$G_c = \left\{ - \left[x \frac{dv_g}{dP} + (1-x) \frac{dv_f}{dP} - \frac{v_{fg}}{s_{fg}} \left(\frac{ds_f}{dP} + x \frac{ds_{fg}}{dP} \right) \right] \right\}^{-0.5}$
	HEM isentropic (b)	$G_c = \left\{ - \left[x \frac{dv_g}{dP} + (1-x) \frac{dv_f}{dP} + (v_g - v_f) \frac{dx}{dP} \right] \right\}^{-0.5}$ where $\frac{dx}{dP} = \frac{v_f + x v_{fg}}{h_{fg}} - x c_{p,g} \frac{T v_{fg}}{h_{fg}^2} - \frac{(1-x)}{h_{fg}} \left[c_{p,f} \frac{T v_{fg}}{h_{fg}} + v_f (1 - \beta T) \right]$
Homogeneous Frozen Model	HFM [18]	$G_c = \left\{ - \left[x \frac{dv_g}{dP} + (1-x) \frac{dv_f}{dP} \right] \right\}^{-0.5}$

Fig. 7. Comparison of predictions of two-phase critical flow models with experimental critical flow data of Fauske [2] through a pipe with a diameter of 3.175 mm for (a) $P_c = 2137$–2489 kPa and (b) $P_c = 1207$–1496 kPa.

$$G_c = \left\{ -\left[x\frac{dv_g}{dP} + (1-x)\frac{dv_f}{dP} + (v_g - v_f)\left(\frac{v_f + xv_{fg}}{h_{fg}} - xc_{p,g}\frac{Tv_{fg}}{h_{fg}^2} - \frac{(1-x)}{h_{fg}}\left(c_{pf}\frac{Tv_{fg}}{h_{fg}} + v_f(1-\beta T) \right) \right) \right] \right\}^{-0.5}. \quad (55)$$

4. Comparison of two-phase critical flow model predictions with experimental critical flow data

Summarized in Table 2 are the two-phase critical flow models presented in the previous sections, which can be grouped into three categories: Slip Flow Models (SFMs), Homogeneous Equilibrium Models (HEMs), and a Homogeneous Frozen Model (HFM). Figs. 7–9 compare two-phase critical flow model predictions with experimental critical flow data for a 3.175-mm diameter pipe [2], short tube orifices with diameters of 1.33 and 1.34 mm

[8], and a short nozzle with a throat diameter of 5.4 mm [11], respectively. Notice that P_c is the pressure at the critical cross-section, and an average of experimental P_c values is used in predictions of the critical flow models.

For pipe flow, the HFM shows good predictions for the low quality region ($x < 0.1$) for high and low pressures, Fig. 7(a) and (b), respectively. Excepting the SFM Fauske simple model, the SFMs show good prediction for the high quality region ($x > 0.1$). The effect of using different relations to evaluate dx/dp in Eq. (41) is investigated by comparing predictions using Eqs. (44), (47) and
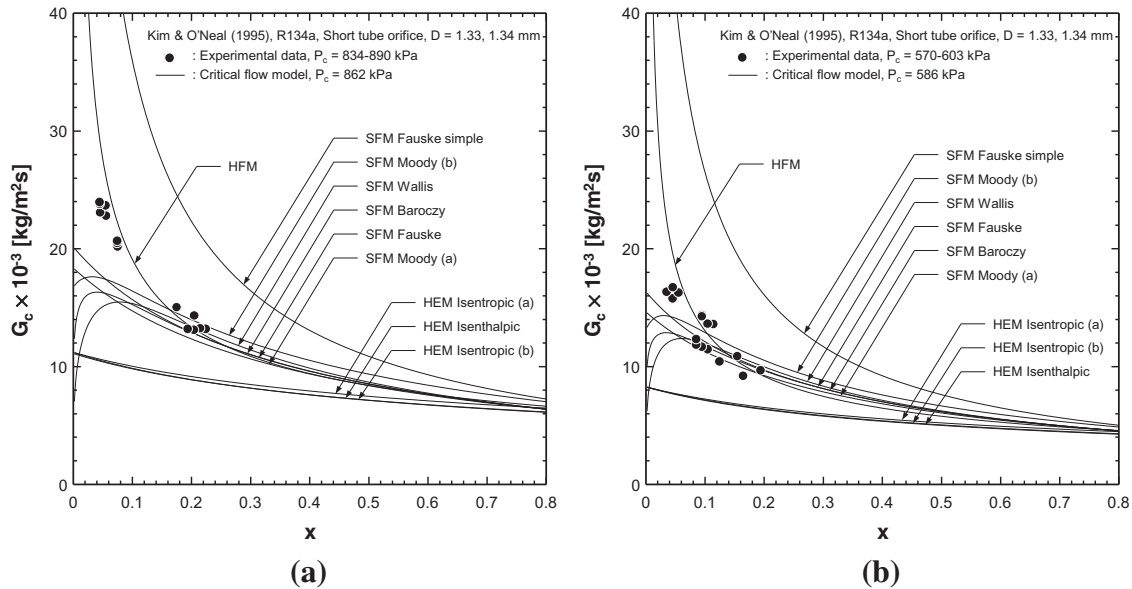
Fig. 8. Comparison of predictions of two-phase critical flow models with experimental critical flow data of Kim and O'Neal [8] for short tube orifices with diameters of 1.33 and 1.34 mm for (a) $P_c = 834$–890 kPa and (b) $P_c = 570$–603 kPa.
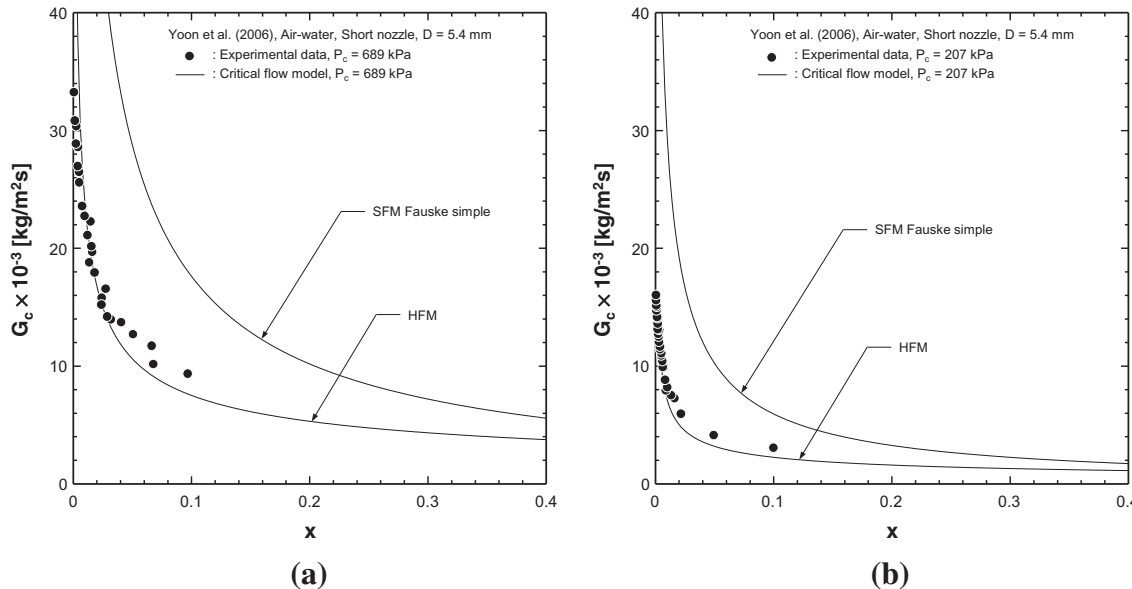
Fig. 9. Comparison of predictions of two-phase critical flow models with experimental critical flow data of Yoon et al. [11] for a short nozzle with a throat diameter of 5.4 mm for (a) $P_c = 689$ kPa and (b) $P_c = 207$ kPa.

(54), corresponding to HEM Isenthalpic, HEM Isentropic (a), and HEM Isentropic (b), respectively. Fig. 7(a) and (b) show all of the HEMs underpredict the experimental data, and different relations for dx/dp have minimal influence on the critical mass velocity.

Fig. 8(a) and (b) compare two-phase critical flow model predictions with experimental critical flow data for short tube orifices [8] for high and low pressures, respectively. The experimental data are highly underpredicted by all HEMs, and highly overpredicted by the SFM Fauske simple. In addition, the low quality region ($x < 0.1$) is underpredicted by most SFMs. Overall, the HFM provides good predictions for both high and low pressures, Fig. 8(a) and (b), respectively.

Fig. 9(a) and (b) compare two-phase critical flow model predictions with experimental critical flow data for air–water in a short nozzle [11] at high and low pressures, respectively. In the absence of mass transfer for air–water flow, $dx/dP = 0$, therefore only the SFM Fauske simple and HFM are examined. The HFM shows good predictions for both high and low pressures, while the SFM Fauske simple highly overpredicts the data for both pressure ranges.

Overall, Figs. 7–9 show that HFM provides the best overall predictive accuracy for the three different flow configurations and different fluids despite its simplicity compared to all other two-phase critical flow models.

5. Comparison of two-phase critical flow model predictions with premature CHF data for micro-channel heat sinks

Fig. 10 compares two-phase critical flow model predictions to experimental mass velocities and qualities corresponding to premature CHF in micro-channel heat sinks by Qu and Mudawar [30] (water, rectangular channels), Fig. 10(a), Koşar et al. [31] (water, rectangular channels), Fig. 10(b), and Wang et al. [32] (water, trapezoidal channels), Fig. 10(c). It should be noted that, in the studies by Koşar et al. and Wang et al., severe pressure oscillation as well as vapor flow reversal into the inlet plenum were observed in the parallel micro-channels, and this behavior was termed by the original authors as Onset of Unstable Boiling (OUB) and unsteady flow boiling, respectively. In all three cases shown in
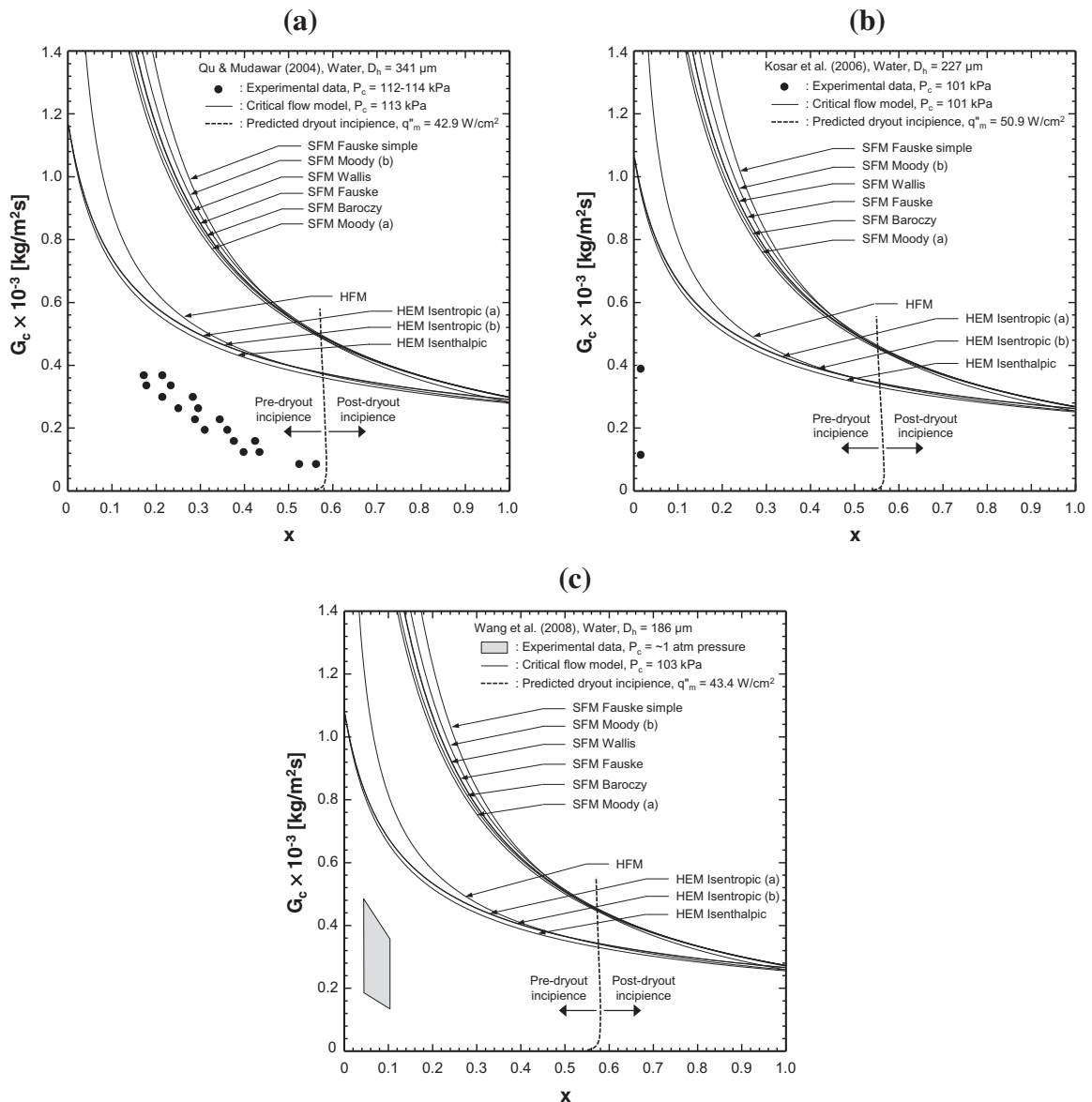

Fig. 10. Comparison of predictions of two-phase critical flow models and Kim and Mudawar's [24] universal dryout incipience quality correlation with experimental premature CHF data in micro-channel heat sinks of (a) Qu and Mudawar [30], (b) Koşar et al. [31] and (c) Wang et al. [32].

Table 3
Universal dryout incipience quality correlation for saturated boiling mini/micro-channel flows [24].

$$x_{di} = 1.4 We_{fo}^{0.03} P_R^{0.08} - 15.0 \left(Bo \frac{P_H}{P_F} \right)^{0.15} Ca^{0.35} \left(\frac{\rho_g}{\rho_f} \right)^{0.06}$$

where $We_{fo} = \frac{G^2 D_h}{\rho_f \sigma}$,

$P_R = \frac{P}{P_{crit}}$, $Bo = \frac{q''_H}{G h_{fg}}$, $Ca = \frac{\mu_f G}{\rho_f \sigma} = \frac{We_{fo}}{Re_{fo}}$,

q''_H: effective heat flux averaged over heated perimeter of channel,
P_H: heated perimeter of channel, P_F: wetted perimeter of channel

Fig. 10(a)–(c), all critical flow models are shown overpredicting the experimental premature CHF data, i.e., premature CHF occurs at mass velocities that are lower than the predicted critical mass velocities. Premature CHF is therefore not the result of two-phase choking.

The same figures compare premature CHF occurrence to that of dryout incipience, which is predicted by the universal dryout incipience quality correlation [24] for saturated flow boiling in mini/micro-channels. Table 3 provides a summary of this correlation based on a combination of dimensionless parameters, which include Weber number, We_{fo}, reduced pressure, P_R (=P/P_{crit}), Boiling number, Bo, ratio of the flow channel's heated to wetted perimeters, P_H/P_F, Capillary number, Ca, and density ratio, ρ_f/ρ_g. Fig. 10(a)–(c) show premature CHF occurs at qualities that are smaller than predicted by the dryout incipience quality correlation.

6. Comparison of two-phase critical flow model predictions with CHF data for micro-channel heat sinks

Fig. 11 compares predictions of the two-phase critical flow models with experimental mass velocities and qualities corresponding to CHF in micro-channel heat sinks by Agostini et al. [33], Fig. 11(a), and Kuo and Peles [34], Fig. 11(b), where CHF corresponds to complete dryout of the annular liquid film. The CHF data of Agostini et al. are overpredicted by all the critical flow models, and those of Kuo and Peles overpredicted by the HFM and SFMs. Notice that some of the CHF data of Kuo and Peles in the

low quality region are underpredicted by the HEMs. However, this result is inconsequential, given that the HEMs underpredict all critical flow data as presented in Figs. 7–9. Fig. 11(a) and (b) also show locations of dryout incipience according to the universal dryout incipience quality correlation [24]. As expected, all the CHF data are located in the post-dryout incipience region that exceeds the quality corresponding dryout incipience.

Fig. 12 compares predictions of the two-phase critical flow models with experimental mass velocities and qualities corresponding to CHF in micro-channel heat sinks at subatmospheric pressures by Kuo and Peles [35]. The micro-channels featured 20-μm wide inlet restrictors and a 400-μm long orifice at the micro-channel inlets to suppress severe pressure oscillation and parallel channel instability that might induce premature CHF. Based on flow visualization studies, Kuo and Peles concluded that CHF was associated with dryout of the annular liquid film at the micro-channel exits. Additionally, they attributed a significant reduction of CHF at very low pressures to compressibility, choking and rarefaction that become increasingly important at low pressures. Fig. 12 shows that as the pressure decreases, the experimental CHF data become underpredicted by the two-phase critical flow models. This is particular the case for 20 kPa, Fig. 12(c), where most of the CHF data are located above the choking line.

In order to examine the relationships among critical flow, premature CHF and CHF in micro-channels, predictions of previous premature CHF and CHF correlations, which are summarized in Table 4, are compared to those of the Homogeneous Frozen Model (HFM) for critical flow. First, dryout incipience is predicted according to the universal dryout incipience quality correlation [24]. The critical mass velocity for premature CHF is predicted by the premature CHF correlation [30] in the pre-dryout incipience region, and CHF by the CHF correlations for water [36] and refrigerants [37] in the post-dryout incipience region. Notice that the premature CHF correlation [30] is based on water data in a rectangular micro-channel heat sink, and the CHF correlation, which was derived from water data [36], has been shown in [37] to yield good predictions of data for R236fa in a rectangular micro-channel heat sink [33]. For water, Fig. 13(a) shows the critical mass velocity corresponding to premature CHF increases with decreasing system pressure, and exceeds the choking line predicted by the HFM for
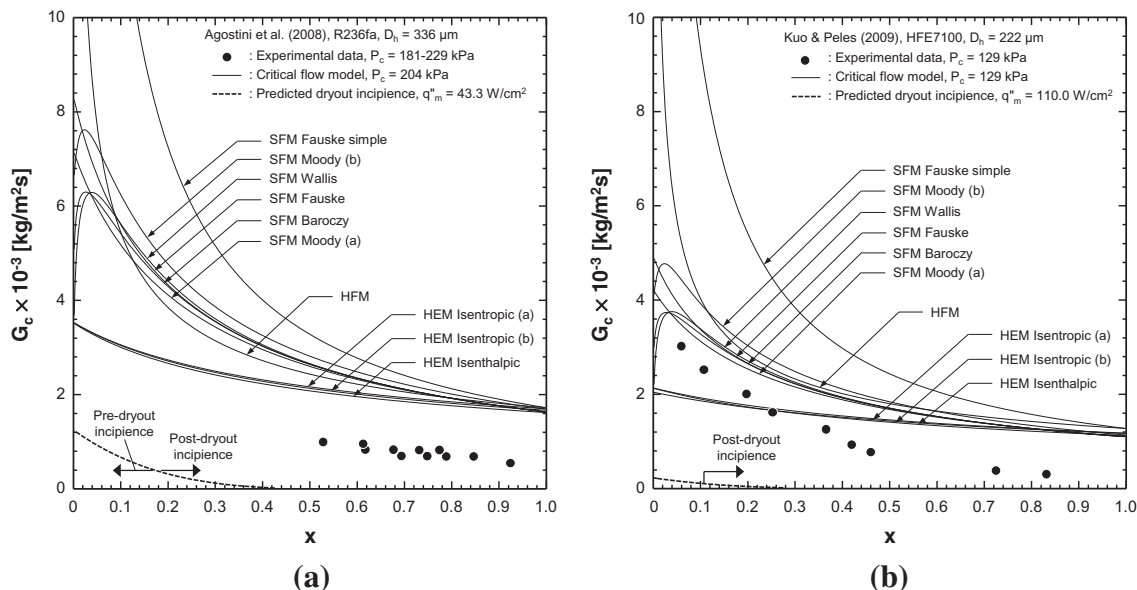

Fig. 11. Comparison of predictions of two-phase critical flow models and Kim and Mudawar's [24] universal dryout incipience quality correlation with experimental CHF data in micro-channel heat sinks of (a) Agostini et al. [33] and (b) Kuo and Peles [34].
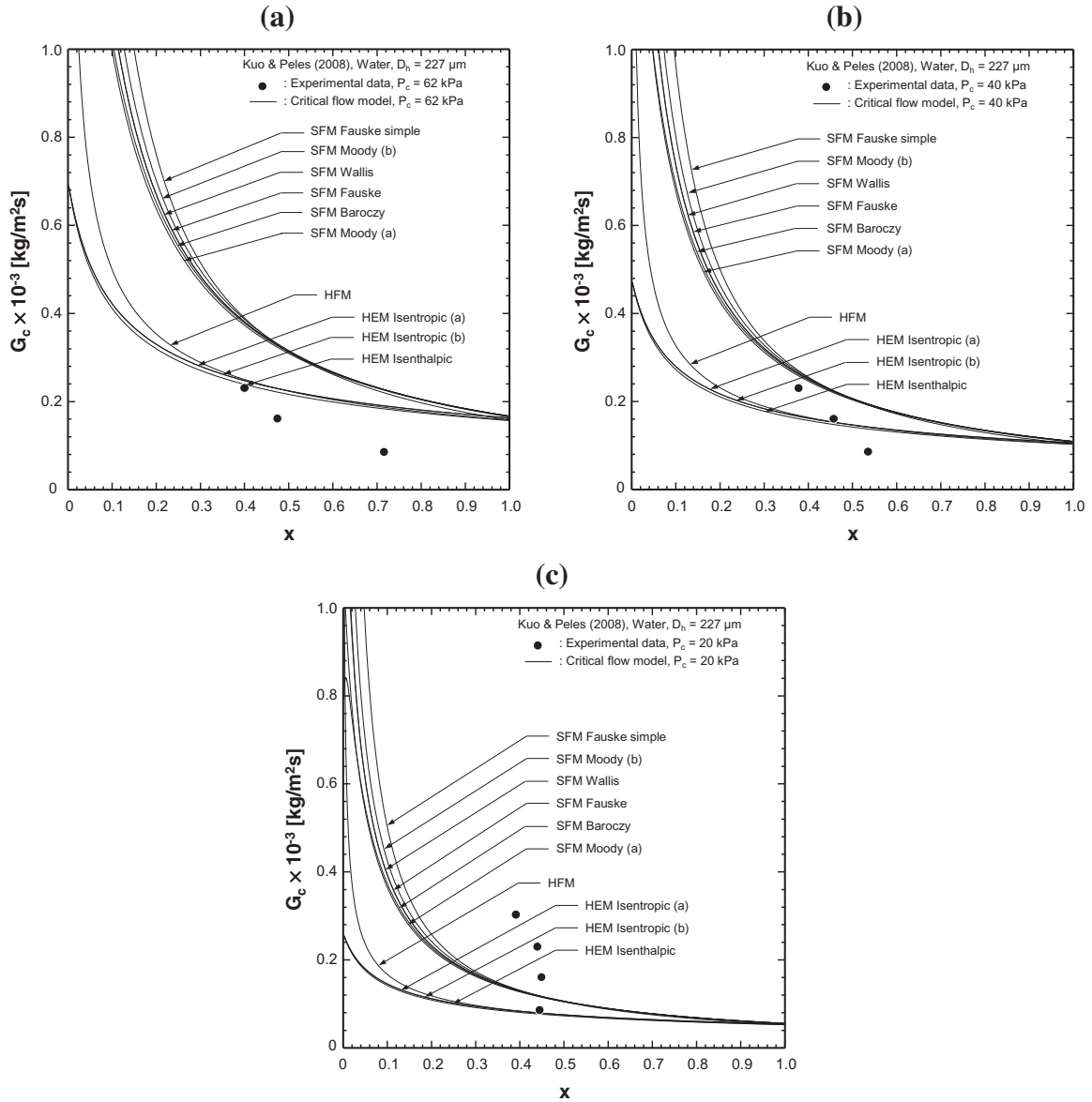
(a)

(b)

(c)

Fig. 12. Comparison of predictions of two-phase critical flow models with experimental CHF data in micro-channel heat sink with inlet restrictors of Kuo and Peles [35] for (a) P_c = 62 kPa, (b) P_c = 40 kPa and (c) P_c = 20 kPa.

Table 4
Premature CHF and CHF correlations.

Authors	Equation[a]	Remarks
Qu and Mudawar [30]	$q'_{P-CHF} = 33.43 G h_{fg} \left(\frac{\rho_g}{\rho_f}\right)^{1.11} We_L^{-0.21} \left(\frac{L}{D_h}\right)^{-0.36}$ where $We_L = \frac{G^2 L}{\rho_f \sigma}$	Premature CHF correlation, D_h = 341 µm for water (three-sided heated), D = 2.54 mm, 510 µm for R113
Sudo et al. [36]	$q'_{CHF} = 0.005 G^{0.611} h_{fg} \left[\rho_g (\rho_f - \rho_g) g \sqrt{\frac{\sigma}{(\rho_f - \rho_g)g}} \right]^{0.1945}$	CHF correlation, two-sided heated rectangular channel with gaps of 2.25, 2.80 mm for water
Wojtan et al. [37]	$q'_{CHF} = 0.437 G h_{fg} \left(\frac{\rho_g}{\rho_f}\right)^{0.073} We_L^{-0.24} \left(\frac{L}{D_h}\right)^{-0.72}$	CHF correlation, D = 509, 790 µm for R134a, R245fa

[a] Heated equivalent diameter was used instead of D_h in [30], and D was used instead of D_h in [37].

P_c = 70 kPa. Fig. 13(b) shows the critical mass velocity for R236fa corresponding to CHF exceeds the choking line for the lowest pressure, P_c = 50 kPa. Also for R236fa, Fig. 13(c) shows the critical mass velocity corresponding to CHF exceeds the choking line for the lowest diameter of D_h = 200 µm. These results prove that premature CHF and CHF can be associated with choking both at low
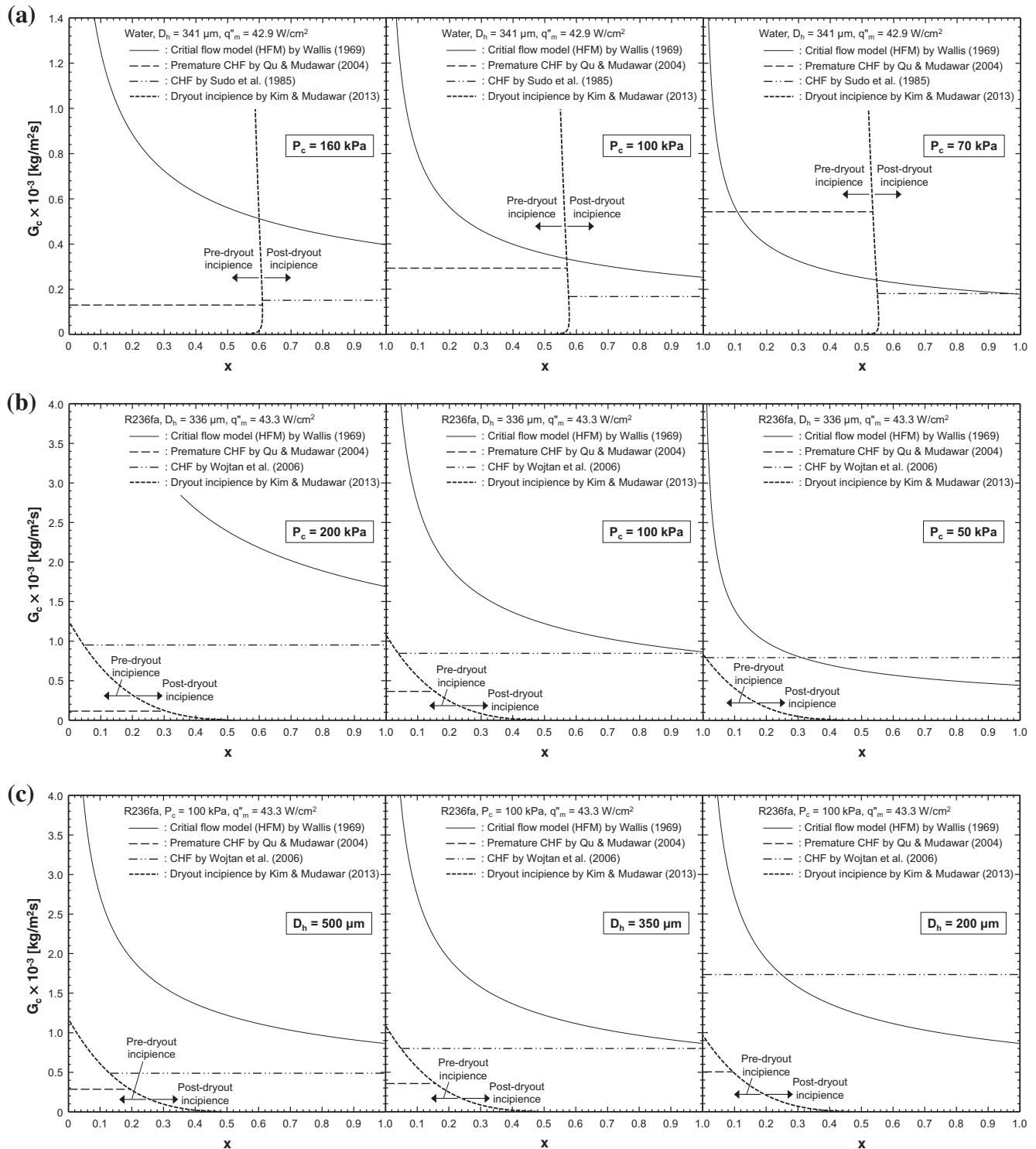
Fig. 13. Comparison of predictions of Homogeneous Frozen Model (HFM) for critical flow [18] with those of correlations for premature CHF [30] and CHF [36,37] for (a) micro-channel water flow at different pressures, (b) micro-channel R236fa flow at different pressures, and (c) micro-channel R236fa flow for different channel diameters. Dryout incipience is predicted by the universal dryout incipience quality correlation [24] for saturated flow boiling in mini/micro-channels.

pressures and in very small channels. These findings support the hypothesis proposed by Bowers and Mudawar [14–16] concerning the likelihood of choking in micro-channel heat sinks.

The results presented in Figs. 7–13 point to important flow and heat transfer limits for saturated flow boiling in micro-channel

heat sinks, which are qualitatively summarized in Fig. 14. Premature CHF and CHF generally fall below the choking line, but begin to exceed the choking line with decreasing pressure or decreasing channel diameter. Fig. 14 also shows premature CHF and CHF are segregated by the dryout incipience quality.
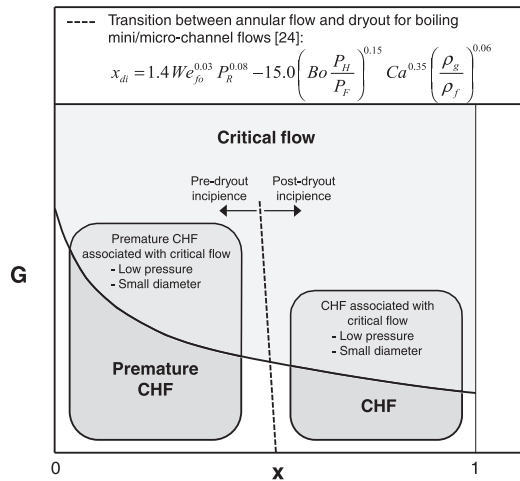
Fig. 14. Qualitative representation of flow and heat transfer limits for saturated flow boiling in micro-channel heat sinks.

7. Conclusions

This study reviewed two-phase critical flow models, which are grouped into Slip Flow Models (SFMs), Homogeneous Equilibrium Models (HEMs), and Homogeneous Frozen Model (HFM). Also discussed is the relationship between choking, premature CHF, and CHF for saturate flow boiling in micro-channel heat sinks. Key findings from the study are as follows:

1. Two-phase critical flow models are compared to previous experimental choking data for flow data through a pipe, short tube orifices, and a short nozzle. Most SFMs show good predictions in the high quality region, while the HFM shows good predictions in the low quality region and both low and high pressures.
2. Two-phase critical flow models are also compared to previous experimental premature CHF and CHF data for micro-channel heat sinks. Premature CHF and CHF generally fall below the choking line, but begin to exceed the choking line and are therefore associated with choking with decreasing pressure or decreasing channel diameter.
3. Premature CHF and CHF are segregated by dryout incipience quality. Premature CHF occurs at quality values below this limit, and CHF above this limit.

Acknowledgments

References

[1] H.S. Isbin, J.E. Moy, A.J.R. Da Cruz, Two-phase, steam-water critical flow, AIChE J. 3 (1957) 361–365.
[2] H.K. Fauske, Contribution to the theory of two-phase, one-component critical flow, Report ANL-6633, Argonne National Lab., Argonne, IL, 1962.
[3] F.J. Moody, Maximum two-phase vessel blowdown from pipes, Report APED-4827, General Electric Co., San Jose, CA, 1965.
[4] W.J. Klingebiel, R.W. Moulton, Analysis of flow choking of two-phase, AIChE J. 17 (1971) 383–390.
[5] M. Deichsel, E.R.F. Winter, Adiabatic two-phase pipe flow of air–water mixtures under critical flow conditions, Int. J. Multiphase Flow 16 (1990) 391–406.
[6] D.W.H. Fraser, A.H. Abdelmessih, A study of the effect of the location of flashing inception on maximum and minimum critical two-phase flow rates: Part I – experimental, Nucl. Eng. Des. 211 (2002) 1–11.
[7] G.L. Sozzi, W.A. Sutherland, Critical flow of saturated and subcooled water at high pressure, Report NEDO-13418, General Electric Co., San Jose, CA, 1975.
[8] Y. Kim, D.L. O'Neal, A comparison of critical flow models for estimating two-phase flow of HCFC22 and HFC134a through short tube orifices, Int. J. Refrig. 18 (1995) 447–455.
[9] J.C. Hesson, Flow of two-phase carbon dioxide through orifices (Ph.D. thesis), Illinois Institute of Technology, Chicago, IL, 1957.
[10] F.W. Bonnet, Critical two-phase flow of nitrogen and oxygen through orifices, Adv. Cryog. Eng. 12 (1967) 427–437.
[11] H.J. Yoon, M. Ishii, S.T. Revankar, Choking flow modeling with mechanical non-equilibrium for two-phase two-component flow, Nucl. Eng. Des. 236 (2006) 1886–1901.
[12] R.E. Henry, A study of one- and two-component, two-phase critical flows at low qualities, Report ANL-7430, Argonne National Lab., Argonne, IL, 1968.
[13] R.J. Simoneau, R.C. Hendricks, Two-phase choked flow of cryogenic fluids in converging–diverging nozzles, Report TP-1484, NASA Lewis Research Center, OH, 1979.
[14] M.B. Bowers, I. Mudawar, Two-phase electronic cooling using mini-channel and micro-channel heat sinks – Part 1. Design criteria and heat diffusion constraints, J. Electron. Packaging – Trans. ASME 116 (1994) 290–297.
[15] M.B. Bowers, I. Mudawar, Two-phase electronic cooling using mini-channel and micro-channel heat sinks – Part 2. Flow rate and pressure drop constraints, J. Electron. Packaging – Trans. ASME 116 (1994) 298–305.
[16] M.B. Bowers, I. Mudawar, High flux boiling in low flow rate, low pressure drop mini-channel and micro-channel heat sinks, Int. J. Heat Mass Transfer 37 (1994) 321–332.
[17] W. Qu, I. Mudawar, Transport phenomena in two-phase micro-channel heat sinks, J. Electron. Packaging – Trans. ASME 126 (2004) 213–224.
[18] G.B. Wallis, One Dimensional Two-phase Flow, second ed., McGraw-Hill, New York, NY, 1969.
[19] A.E. Bergles, Review of instability in two-phase systems, in: S. Kakac, F. Mayinger (Eds.), Two-phase Flows and Heat Transfer, vol. 1, Hemisphere, Washington, DC, 1977, pp. 383–422.
[20] G. Yadigaroglu, Two-phase flow instabilities and propagation phenomena, in: J.M. Delhaye, M. Giot, M.L. Riethmuller (Eds.), Thermohydraulics of Two-phase Systems for Industrial Design and Nuclear Engineering, Hemisphere, Washington, DC, 1981, pp. 353–403.
[21] W. Qu, I. Mudawar, Measurement and prediction of pressure drop in two-phase micro-channel heat sinks, Int. J. Heat Mass Transfer 46 (2003) 2737–2753.
[22] J. Lee, I. Mudawar, Fluid flow and heat transfer characteristics of low temperature two-phase micro-channel heat sinks – Part 1: experimental methods and flow visualization results, Int. J. Heat Mass Transfer 51 (2008) 4315–4326.
[23] J. Lee, I. Mudawar, Two-phase flow in high-heat-flux micro-channel heat sink for refrigeration cooling applications: Part II – heat transfer characteristics, Int. J. Heat Mass Transfer 48 (2005) 941–955.
[24] S.M. Kim, I. Mudawar, Universal approach to predicting saturated flow boiling heat transfer in mini/micro-channels – Part I. Dryout incipience quality, Int. J. Heat Mass Transfer 64 (2013) 1226–1238.
[25] C.J. Baroczy, Correlation of liquid fraction in two-phase flow with applications to liquid metals, Chem. Eng. Prog. 61 (1965) 179–191.
[26] R.W. Lockhart, R.C. Martinelli, Proposed correlation of data for isothermal two-phase, two-component flow in pipes, Chem. Eng. Prog. 45 (1949) 39–48.
[27] F.J. Moody, Maximum flow rate of a single component, two-phase mixture, J. Heat Transfer – Trans. ASME 87 (1965) 134–141.
[28] S.M. Zivi, Estimation of steady-state steam void-fraction by means of the principle of minimum entropy production, J. Heat Transfer – Trans. ASME 86 (1964) 247–252.
[29] R.T. Lahey, F.J. Moody, The Thermal Hydraulics of a Boiling Water Nuclear Reactor, American Nuclear Society, Hinsdale, IL, 1977.
[30] W. Qu, I. Mudawar, Measurement and correlation of critical heat flux in two-phase micro-channel heat sinks, Int. J. Heat Mass Transfer 47 (2004) 2045–2059.
[31] A. Koşar, C.J. Kuo, Y. Peles, Suppression of boiling flow oscillations in parallel microchannels by inlet restrictors, J. Heat Transfer – Trans. ASME 128 (2006) 251–260.
[32] G. Wang, P. Cheng, A.E. Bergles, Effects of inlet/outlet configurations on flow boiling instability in parallel microchannels, Int. J. Heat Mass Transfer 51 (2008) 2267–2281.
[33] B. Agostini, R. Revellin, J.R. Thome, M. Fabbri, B. Michel, D. Calmi, U. Kloter, High heat flux flow boiling in silicon multi-microchannels – Part III: saturated critical heat flux of R236fa and two-phase pressure drops, Int. J. Heat Mass Transfer 51 (2008) 5426–5442.
[34] C.J. Kuo, Y. Peles, Flow boiling of coolant (HFE-7000) inside structured and plain wall microchannels, J. Heat Transfer – Trans. ASME 131 (2009) 121011.
[35] C.J. Kuo, Y. Peles, Critical heat flux of water at subatmospheric pressures in microchannels, J. Heat Transfer Trans. ASME 130 (2008) 072403.
[36] Y. Sudo, K. Miyata, H. Ikawa, M. Kaminaga, M. Ohkawara, Experimental study of differences in DNB heat flux between upflow and downflow in vertical rectangular channel, J. Nucl. Sci. Technol. 22 (1985) 604–618.
[37] L. Wojtan, R. Revellin, J.R. Thome, Investigation of saturated critical heat flux in a single, uniformly heated microchannel, Exp. Therm. Fluid Sci. 30 (2006) 765–774.